Structure and Properties of Tethered Bilayer Lipid Membranes with Unsaturated Anchor Molecules

ARTICLE *in* LANGMUIR · JUNE 2013

Impact Factor: 4.46 · DOI: 10.1021/la401132c · Source: PubMed

12 AUTHORS, INCLUDING:

Rima Budvytyte
University of Copenhagen
25 PUBLICATIONS **211** CITATIONS
SEE PROFILE

Frank Heinrich
Carnegie Mellon University
52 PUBLICATIONS **644** CITATIONS
SEE PROFILE

Sidd Shenoy
Carnegie Mellon University
16 PUBLICATIONS **92** CITATIONS
SEE PROFILE

David J Vanderah
Institute for Bioscience and Biotechnology Re…
90 PUBLICATIONS **1,859** CITATIONS
SEE PROFILE

Langmuir

Article

pubs.acs.org/Langmuir

Structure and Properties of Tethered Bilayer Lipid Membranes with Unsaturated Anchor Molecules

Rima Budvytyte,[†] Gintaras Valincius,[†] Gediminas Niaura,[†] Vladislava Voiciuk,[†,○] Mindaugas Mickevicius,[†] Hilary Chapman,[‡,§] Haw-Zan Goh,[∥] Prabhanshu Shekhar,[∥] Frank Heinrich,[∥,#] Siddharth Shenoy,[∥] Mathias Lösche,[⊥,∥,#] and David J. Vanderah*[,‡,▽]

[†]Institute of Biochemistry, Vilnius University, Vilnius LT-08662, Lithuania

[‡]Material Measurement Laboratory and [#]Center for Neutron Research, National Institute of Standards and Technology, Gaithersburg, Maryland 20899, United States

[§]Hood College, Frederick, Maryland 21701, United States

[∥]Physics Department and [⊥]Department of Biomedical Engineering, Carnegie Mellon University, Pittsburgh, Pennsylvania 15213, United States

[▽]Institute for Bioscience and Biotechnology Research, Rockville, Maryland 20850, United States

Supporting Information

ABSTRACT: The self-assembled monolayers (SAMs) of new lipidic anchor molecule HC18 [*Z*-20-(*Z*-octadec-9-enyloxy)-3,6,9,12,15,18,22-heptaoxatetracont-31-ene-1-thiol] and mixed HC18/*β*-mercaptoethanol (*β*ME) SAMs were studied by spectroscopic ellipsometry, contact angle measurements, reflection−absorption infrared spectroscopy, and electrochemical impedance spectroscopy (EIS) and were evaluated in tethered bilayer lipid membranes (tBLMs). Our data indicate that HC18, containing a double bond in the alkyl segments, forms highly disordered SAMs up to anchor/*β*ME molar fraction ratios of 80/20 and result in tBLMs that exhibit higher lipid diffusion coefficients relative to those of previous anchor compounds with saturated alkyl chains, as determined by fluorescence correlation spectroscopy. EIS data shows the HC18 tBLMs, completed by rapid solvent exchange or vesicle fusion, form more easily than with saturated lipidic anchors, exhibit excellent electrical insulating properties indicating low defect densities, and readily incorporate the pore-forming toxin *α*-hemolysin. Neutron reflectivity measurements on HC18 tBLMs confirm the formation of complete tBLMs, even at low tether compositions and high ionic lipid compositions. Our data indicate that HC18 results in tBLMs with improved physical properties for the incorporation of integral membrane proteins (IMPs) and that 80% HC18 tBLMs appear to be optimal for practical applications such as biosensors where high electrical insulation and IMP/peptide reconstitution are imperative.

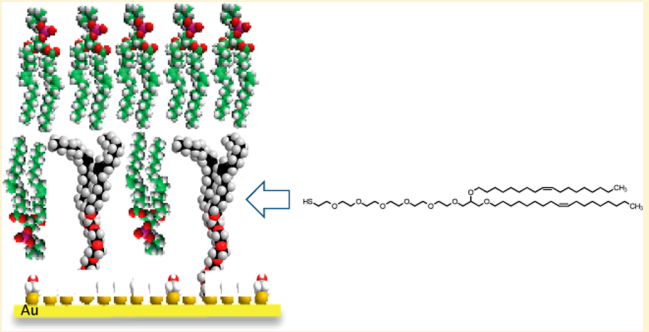

INTRODUCTION

Many advances in our understanding of the physical properties, structure, and function of biomembranes have been achieved with membrane mimics such as solid-supported membranes (SSMs) and tethered bilayer lipid membranes (tBLMs). SSMs, first reported by Brian and McConnell, readily assemble on Si or glass substrates,[1,2] exhibit limited stability with no control over the space between membrane and substrate that may impede the functional reconstitution of membrane proteins,[3] or lead to the denaturation of the incorporated protein through direct contact between extramembraneous protein domains and the underlying substrate.[4]

Bilayers tethered to a surface by hydrophilic segments or low-molecular-weight polymers,[5−14] tBLMs, are an alternative to SSMs that exhibit improved stability and are being increasingly used as experimental platforms for studies of reconstituted membrane proteins[15−23] and sensors[10,24−26] that range from the detection of biological agents to pharmaceutical screening. In addition, tBLMs can directly address membrane-support proximity problems through tether/polymer design.

Within a broad range of structural possibilities, we have focused on tBLMs tethered to planar Au films via 1-mercapto(ethylene oxide)$_n$ [HS(CH$_2$CH$_2$O)$_n$, HS(EO)$_n$, n = 6 to 9; 1-mercapto(EO)$_n$] segments, laterally diluted on the Au surface by coadsorption with *β*-mercaptoethanol (*β*ME).[7,27,28] These 1-mercapto(EO)$_n$ oligomers are covalently linked to a dual-chain glycerol-based lipidic motif that intercalates into the bilayer leaflet proximal to the substrate, ligating the membrane to the solid surface. After the initial formation of a mixed self-assembled monolayer (SAM) of the tether lipid and *β*ME,

Received: March 27, 2013
Revised: June 6, 2013
Published: June 7, 2013

membrane completion is achieved either by the precipitation of a dissolved phospholipid (lipid mixture) on the SAM by rapid solvent exchange (RSE)[7,24] or by vesicle adsorption and fusion. Similar systems have been developed by others.[29−31] The physical properties of the tBLM constructs can be controlled by the mixed SAM tether lipid/βME ratio, which in turn determines the rigidity of the proximal bilayer leaflet.[7,32] SAMs of only tether lipids at the surface lead to tBLMs with excellent membrane resistances (Table 4 in ref 7); however, bilayer systems densely packed with molecules anchored to the substrate may pose problems for the functional reconstitution of proteins.[33] However, tBLMs in which the tether lipids are diluted with βME show (a) membrane resistances only slightly reduced from that measured for fully tethered membranes, (b) full fluidity of the distal phospholipid layers, and (c) only modestly reduced lipid diffusion in the proximal layers.[32] These tBLMs have been shown to accommodate reconstituted proteins such as the exotoxin α-hemolysin (αHL) at high concentrations in a functional state.[19,22,34]

In addition to the lateral dilution of the tether compound on the substrate, the physical properties of tBLM systems will depend on the untethered lipids and the tether compound, the hydrophobic alkyl, and the hydrophilic tether segments. Although unsaturated lipids such as 1-palmitoyl-2-oleoyl-*sn*-glycero-3-phosphocholine (POPC) and 1,2-dioleoyl-*sn*-glycero-3-phospho-choline (DOPC) have been used in the completion of tBLMs,[27] the effects of unsaturation in the tBLM tether compounds remain to be explored. In the current work, we characterize tBLMs using a new lipidic anchor molecule, HC18 [(*Z*-20-(*Z*-octadec-9-enyloxy)-3,6,9,12,15,18,22-heptaoxatetracont-31-ene-1-thiol, (C_{18} = oleoyl)] (Scheme 1), containing

Scheme 1. Structures of Lipidic Tether Compounds

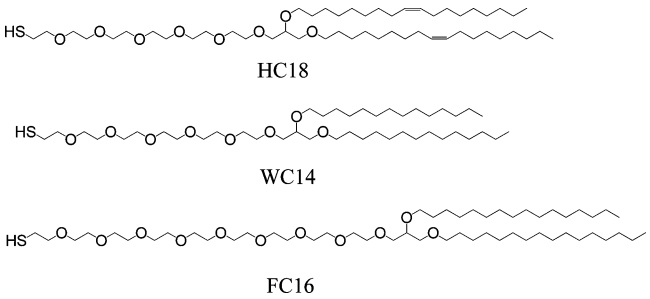

one carbon−carbon double bond in each of the hydrophobic chains and demonstrate the formation of tBLMs with high electrical resistance and dynamic lateral diffusion, with high concentrations of anionic lipids, improved tBLM completion with vesicle fusion, and the reconstitution of αHL under conditions not observed with saturated chain tethers WC14 [20-tetradecyloxy-3,6,9,12,15,18,22-heptaoxahexatricontane-1-thiol, C_{14} (myristoyl)][7] and FC16 [29-hexadecyloxy-3,6,9,12,15,18,21,24,27,31-decaoxaheptatetracontan-1-thiol, C_{16}, palmitoyl].[27]

MATERIALS AND METHODS[35]

Hexa(ethylene oxide), oleyl alcohol (*Z*-octadec-9-enol, 85%), and thiolacetic acid were purchased from Sigma-Aldrich Chemical Co. (Milwaukee, WI) and used without further purification. Tetrahydrofuran (THF) (Mallinckrodt, AR or North Strong Scientific, Phillipsburg, NJ) was distilled from calcium hydride immediately before use. All other solvents (AR grade) were used without purification, and all reactions were carried out under nitrogen. Lipids POPC, DOPC, 1,2-diphytanoyl-*sn*-glycero-3-phosphocholine (DPhyPC), 1-palmitoyl-2-oleoyl-*sn*-glycero-3-phospho-(1′-*rac*-glycerol) (sodium salt) (POPG), and 1-palmitoyl (d_{31})-2-oleoyl-*sn*-glycero-3-phosphocholine (POPC-d_{31}) were purchased from Avanti Polar Lipids, Inc. (Alabaster, AL) and used as received.

Materials Synthesis. New lipidic anchor molecule HC18 was synthesized as generally outlined for WC14 (Scheme 1 in ref 7 and Supporting Information) with the following modifications: (1) oleyl bromide, prepared from oleyl alcohol (chlorotrimethylsilane-LiBr/CH_3CN,[36] 83%), was used in the conversion of IV to V, (2) corresponding VII was a mesylate ($ClSO_2CH_3$/$(C_2H_5)_3N$, 93%), (3) conversion to HC18 from the corresponding VII mesylate was carried out in two steps, (a) 1.5 eq of $CH_3COS^-Na^+$/MeOH, ∼90% and (b) 0.1 mol/L HCl/MeOH, reflux 8 h, ∼92%.

Sample Preparation. *SAM/Mixed SAM Preparation.* For all substrates other than the neutron reflectometry measurements, NOCHROMIX-cleaned silicon (100) wafers (Silicon, Inc., Boise, ID) were initially coated with chromium (∼2 nm) and then with Au (∼100 nm) by magnetron sputtering (Edwards Auto 306, U.K.). The freshly coated Au wafers were immediately immersed in ethanolic solutions of either the pure tether compound (HC18, WC14, or FC16) or various mole fraction mixtures of HC18, WC14, or FC16, and βME (c_{total} = 0.2 mmol/L), expressed hereafter as *x*% where *x* is the mole fraction of the tether compound × 100). For the neutron reflectivity experiments, 76.2 mm (3.0 in.) diameter × 5 mm thick, phosphorus-doped silicon wafers (El-Cat, Inc., Waldwick, NJ) were sequentially coated with Cr (3 nm) and Au (15 nm) using a Denton Discovery 550 sputtering instrument (Denton Vacuum LLC, Moorestown). Film thickness uniformity was better than 3% over the diameter of the wafer. Exposure of these films to ethanolic solutions of *x*% HC18 for ∼12 h was identical to that just described.

tBLM Preparation. For tBLMs completed with RSE, lipid mixtures of the desired bilayer composition were dissolved in organic solvents at a concentration of 2.5 mg/mL. Zwitterionic lipid mixtures were dissolved in ethanol, and mixtures containing anionic lipids were dissolved in a mixture of 95% methanol, 4% chloroform, and 1% water by volume. SAM/mixed SAM-coated wafers were exposed to the lipid solution for 5 min, and thereafter the organic lipid solution was rapidly replaced by buffer (the RSE method). Buffers for tBLMs prepared with RSE contained 10 mM Na_2HPO_4 and 100 mM NaCl adjusted to pH 7.4 using diluted HCl solution.

For tBLMs completed with vesicle fusion, vesicles were prepared from 2.5 mg of lipid-dried films of the desired lipid composition. Lipids were suspended in 1 mL of buffer and sonicated until the solution became clear. The vesicles were extruded at least 13 times using a manual extruder (Avanti Polar Lipids, Inc., Alabaster, AL) equipped with two 100 nm filters. For vesicle fusion, the vesicles were diluted to a final concentration of 1 mg/mL and kept at room temperature. Silicon wafers coated with the mixed tether/βME SAMs were exposed to the vesicle solution for 1 h and then rinsed with buffer. Buffers for the preparation and measurement of tBLMs completed by vesicle fusion were 50 mM K_2HPO_4 adjusted to pH 7.45 using HCl solution.

Electrochemical Impedance Spectroscopy (EIS). EIS measurements were performed using a Solartron (Farnborough, U.K.) system (1287A potentiostat and 1260 frequency response analyzer) using a Parstat 2273 (Princeton Applied Research, TN) with Power Suite software between 0.1 Hz and 100 kHz, with 10 logarithmically distributed measurement points per decade. Data were fitted using ZView software (Scribner Associates, Southern Pines, NC). The Au-coated wafers (20 mm × 40 mm) served as the working electrodes in a setup that allowed simultaneous EIS measurements in six separate electrochemical cells (volume, $V \approx 290$ μL) on each wafer, with the working surface area $A_{el} \approx 0.32$ cm^2 exposed to the solution. EIS data were normalized to the geometric surface area A_{el}. The roughness factor was ∼1.39, estimated from the gold surface oxidation/oxide stripping charge. A saturated silver−silver chloride [Ag/AgCl/NaCl (aq, sat)] microelectrode (M-401F, Microelectrodes, Bedford, NH) was used as a reference and has a potential of +196 mV versus the standard hydrogen electrode. The auxiliary electrode was a 0.25-mm-

dx.doi.org/10.1021/la401132c | *Langmuir* 2013, 29, 8645−8656

diameter platinum wire (99.99% purity, Aldrich) coiled around the barrel of the reference electrode. Measurements were carried out with 10 mV alternating current at 0 V bias versus the reference electrode in aerated solutions.

Spectroscopic Ellipsometry (SE). SE data were collected on a Woollam M2000D ellipsometer (J. A. Woollam Co., Inc., Lincoln, NE) between 193 and 1000 nm aligned at a nominal angle of incidence of ~70° from the surface normal. Calculations, including ellipsometric (optical) thickness and the exact angle of incidence, were made using vendor-supplied software (WVASE). The reported SE thicknesses are the averages of at least four measurements on each sample wafer as a Cauchy layer built point-by-point on the optical constants of a clean, dry Au surface [successively treated with UV-ozone (15 min), water (15 min for complete removal of gold oxide layers), and finally dried (N_2)].

Contact Angle (CA) Measurements. Advancing water contact angles (CAs) were measured on a camera-based system (First 10 Angstroms, Portsmouth, VA) with vendor-supplied image capture and analysis software using the same substrates as those used in the SE measurements. Each reported CA is the average of three drops on each substrate (standard deviation ±1°).

Reflection–Absorption IR Spectroscopy (RAIRS). RAIRS spectra were recorded on a Vertex 80v FT-IR spectrometer (Bruker, Inc., Leipzig, Germany) equipped with a liquid-nitrogen-cooled MCT narrow band detector and a horizontal reflection accessory. The spectral resolution was set at 4 cm^{-1}. Spectra were acquired from 400 scans at a grazing angle of 80° by using p-polarized light. The sample chamber and the spectrometer were evacuated during the measurements. The spectrum of a SAM of hexadecanethiol-d_{33}, HS-$(CD_2)_{15}CD_3$, on Au was used as a reference. Parameters of the bands were determined by fitting the experimental contour to Gaussians using GRAMS/AI 8.0 (Thermo Scientific) software.

Neutron Reflectivity (NR) Measurements and Data Analysis. NR measurements were performed at the NG1 and AND/R reflectometers at the NIST Center for Neutron Research.[37] Each tBLM sample was measured in three isotopically distinct solvent compositions of either D_2O-based buffer, H_2O-based buffer, or a mixture of the both with a neutron scattering length density (nSLD) of $\rho_n \approx 4 \times 10^{-6}$ $Å^{-2}$, referred to as CM4. The stability of the tBLMs permits solvent composition exchanges in situ on the instrument; therefore, measurements were made on one physical sample, ensuring that the SiO_x/Cr/Au surface layers on the 76.2 mm (3 in.) Si wafers, which dominate the neutron interference patterns in the data, contribute in the same way to the overall data structure in subsequent measurements.

Because of the loss of phase information of the neutron scattering experiment, data evaluation proceeds by fitting the experimental results with models of the surface structure. We recently developed techniques[28] to evaluate bilayer structures at interfaces with composition-space models[38,39] that parameterize the interface structure in terms of chemical compositions and connectivity and yield distributions of submolecular components across the interfacial region. Among other structural properties, this approach provides the density of lipid molecules within the bilayer of a tBLM (i.e., the (average) area per phospholipid, A_0). These results may be directly compared to lipid densities in vesicle membranes or fully hydrated multibilayer samples.[40,41] In addition, the contrast-variation approach using isotopically distinct solvent compositions permits the determination of the bilayer completeness and the water distribution throughout the sample with high precision. Reflectivity curves were fitted using ga_refl software.[42] Confidence limits of the model parameter values were evaluated by Monte Carlo resampling[27] of the data based upon the error bars of the individual data points and are reported as 68% confidence intervals.

Fluorescence Correlation Spectroscopy (FCS). FCS spectra were obtained on tBLMs prepared with 5×10^{-3} mol % lissamine-rhodamine-DOPE (LR-DOPE) admixed with the DOPC solutions using a custom-built two-photon FCS system[32] consisting of a Verdi 10 W continuous wave DPSS laser (λ = 532 nm) that pumps a Mira 900F mode-locked titanium–sapphire laser (125 fs pulse width, 76 MHz repetition rate, 1.8 W at λ = 780 nm) from Coherent (Santa Clara, CA). The output wavelength from the titanium–sapphire laser can be tuned between 700 and 980 nm, and λ = 840 nm is used to excite the lissamine–rhodamine-labeled lipids. A neutral density (ND) filter attenuates the IR output to 5–10 mW before it enters the reflector turret of an Axiovert 200 M inverted microscope (Carl Zeiss, Jena, Germany). The light then passes through a dichroic mirror (750dcspxr; Chroma Technologies, Rockingham, VT) and is focused using a 63× 1.2 NA C-Apochromat water-immersion lens (Carl Zeiss) corrected for the coverslip thickness (0.14 to 0.18) mm. The fluorescence is epi-collected, passed through a bandpass filter (et575/50m-2p, Chroma Technologies), focused via the microscope tube lens, recollimated via an achromatically corrected doublet lens, split into two beams with a 50/50 beam-splitter cube (Thorlabs, NJ), and focused via two achromatically corrected doublet lenses onto two separate avalanche photodiode detectors (SPCM-AQR14, Perkin-Elmer, Fremont, CA). The signal from the detectors is correlated in a hardware correlator (5000EPP, ALV, Langen, Germany).

Fluorescence autocorrelation spectra of labeled lipids diffusing in the plane of the tBLMs were acquired by scanning the interfacial films across the waist of the laser focus in z scans and were analyzed to determine the lipid diffusion constant, D, as described previously.[32,43]

Reconstitution of αHL. DPhyPC-completed 80% and 20% HC18- and WC14-tBLMs were monitored by EIS before and after exposure to αHL (140 nM) at room temperature for 60 min. The 80% tBLMs were completed by vesicle fusion, and the 20% compositions were completed by RSE because the vesicle-fused 20% tBLMs were too defective to be detected by EIS.

RESULTS

SE and Advancing Contact Angle (CA) of HC18/βME SAMs. Spectroscopic ellipsometric thickness (d) and advancing contact angle (CA) data of mixed HC18/βME SAMs as a function of increasing HC18 mol fraction are shown in Figure 1. As can be seen, the SE and CA data show parallel trends.

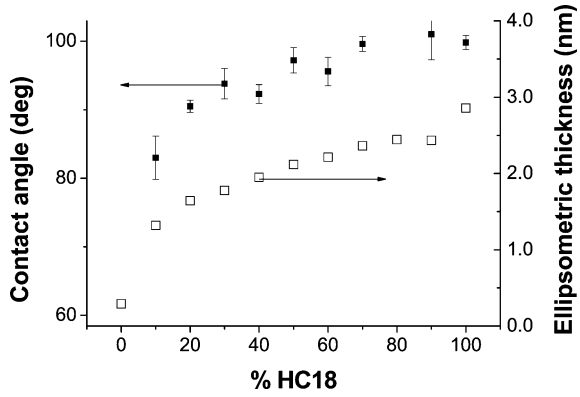

Figure 1. SE thickness (□) and advancing CAs (■) of HC18/βME SAMs from 0 to 100% HC18. The CA value for 100% βME SAM is <10 ± 5° (ref 7).

From 0 to 20%, the d and CA values increase rapidly to ~1.6 nm and ~90°, respectively, leveling off thereafter. A comparison of the HC18 SE and CA data to that of WC14 is informative (Figure 1 and Table 1 in ref 7). The HC18 SAMs are thicker than the WC14 SAMs from 0 to 60% and thinner at all higher compositions, contrary to what might be expected from the longer oleoyl chains in HC18. The CA data exhibit an analogous transition. The $CAs_{(HC18)}$ are smaller than the $CAs_{(WC14)}$ at lower compositions and greater than the $CAs_{(WC14)}$ at higher compositions, with approximately equal values of ~30% (Figure S1 in the Supporting Information section).

dx.doi.org/10.1021/la401132c | Langmuir 2013, 29, 8645–8656

Electrochemical Impedance Spectroscopy (EIS) of Tether/βME SAMs. EIS results of HC18/βME SAMs with direct comparison to those of WC14/βME and FC16/βME are shown in Figure 2A (30%) and 2B (70%). Figure 2A shows that

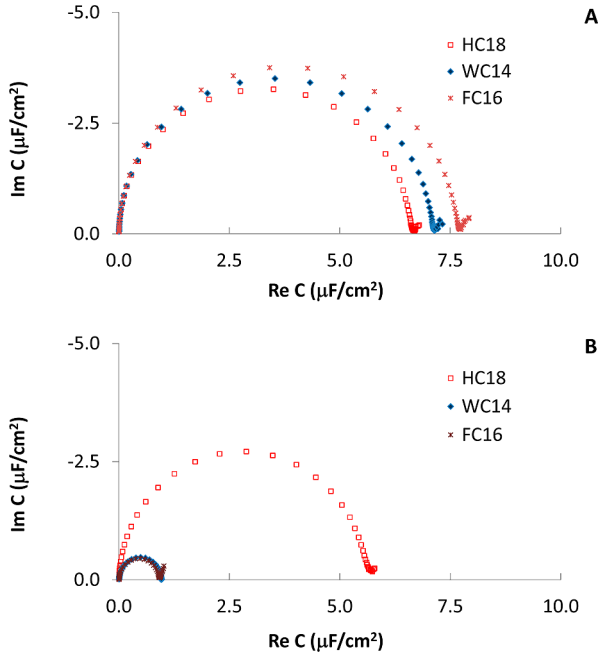

Figure 2. EIS spectra of HC18, WC14, and FC16 SAMs: (A) 30% SAMs and (B) 70% SAMs. Data were obtained on the same-batch SAM-coated, Au-sputtered Si wafers precluding any spectral differences due to surface roughness or other preparation parameters.

all SAMs exhibit nearly perfect semicircular complex capacitance plots with the HC18/βME SAMs exhibiting slightly lower capacitance values. At 70%, the EI spectra of the HC18 SAMs differ drastically from those of WC14 and FC16. Although WC14 and FC16 produce low-capacitance SAMs of ~1 $\mu F/cm^2$, the HC18 SAMs exhibit about 7-fold higher capacitance values that do not differ significantly from those of the 30% HC18 SAMs. EI spectra at ≥80% HC18 SAM compositions were comparable to that for the 70% HC18 SAMs (data not shown).

Reflection Absorption Infrared Spectroscopy (RAIRS) Spectra of Tether/βME SAMs. Figure 3 shows the RAIRS spectral features of 20 to 100% SAMs in the C−H stretching region [Figure 3A (HC18), 3C (WC14), and 3E (FC16)] and in the midrange region [Figure 3B (HC18), 3D (WC14), and 3F (FC16)]. In the C−H stretching region, bands at around 2928 ± 1 and 2858 ± 1 cm^{-1}, assigned to the methylene asymmetric, ν_a, and symmetric, ν_s, vibrations, respectively,[44] dominate at the lower tether compositions, whereas the bands at 2966 ± 1 and 2878 ± 1 cm^{-1}, assigned to the methyl asymmetric, ν_a (IP), and symmetric, ν_s (FR), stretches, respectively,[44] become more prominent as the tether composition increases for all three tether compounds. It is noteworthy that the position of the methylene ν_a band is ≥2920 cm^{-1}, appearing at 2923 cm^{-1} for HC18 (Figure 3A), 2921 cm^{-1} for WC14 (Figure 3C), and 2920 cm^{-1} for FC16 (Figure 3E) in the 100% SAMs (top spectra). In the midrange region [Figure 3B (HC18), 3D (WC14), and 3E (FC16)], an intense absorption band is found in the range from 1050 to 1150 cm^{-1} at all but the lowest of tether compositions, accompanied by higher-wavenumber shoulders of variable intensity. Assigned as the EO asymmetric stretching vibration, ν_{as}(C−O−C),[45−47] the position of this band as an indicator of order in the EO segment[46−52] will be discussed subsequently.

Electrochemical Impedance Spectroscopy (EIS) of HC18 tBLMs. The electrochemical impedance (EI) spectral changes that occur upon RSE of an ethanolic DOPC solution with buffer in the presence of HC18 monolayers are consistent with the formation of bilayers on the anchor SAMs. Complex capacitance plots of the EI spectra as a function of the HC18 composition are shown in Figure 4. In all cases, the semicircular part of the EI spectra sharply decrease (compare Figure 4A,B to Figure 2). After RSE, the high-frequency semicircular arch now points to values spanning from ~0.7 to ~0.8 $\mu F/cm^2$ depending on the tether/βME ratio (Figure 4A), more clearly exemplified in the expanded high-frequency part of the EI spectra (Figure 4B). Taking into account the surface roughness factor of 1.39, such capacitance values are commensurate with the formation of an ~3-nm-thick dielectric layer with a relative dielectric constant of ~2.0 to ~2.3 over a Helmholtz layer with ~8 $\mu F/cm^2$ capacitance. This dielectric constant range is lower than that obtained for WC14 tBLMs RSE-completed with DOPC (~2.8).[16]

At all HC18 compositions, the high-frequency (leftmost) parts of the complex capacitance spectra are similar. As the HC18 composition decreases, the plots begin to exhibit different characteristics as the frequency decreases. At 50% HC18, the midfrequency extremum of the spectrum no longer returns to the x axis and the semicircular diameter is larger than that of the >50% HC18 tBLMs. At compositions <50% HC18, the midfrequency extrema continue to lift off the x axis (Figure 4B), and the spectra exhibit low-frequency tails that increase in length and approximate additional features. The 20 and 10% spectra (Figure 4A) show the emergence of a third semicircular feature.

HC18 and WC14 tBLMs by Vesicle Fusion. We compared the propensities of the HC18 and the WC14 SAMs to form membranes by fusion with DOPC vesicles. The exposure of 20 and 80% SAMs of each tether to DOPC vesicle solutions gave the EI spectra shown in Figure 5. For the 80% SAMs, fusion resulted in the formation of a complete high-frequency semicircular feature (i.e., midfrequency extremum Im C ≈ 0) in the EI spectra. However, vesicle-fused 20% HC18 and WC14 tBLMs exhibit EI spectra more closely resembling those of the corresponding SAMs (Figure 2), showing only the emergence of a high-frequency semicircular feature indicating the inability to form intact tBLMs at this tether composition.

Fluorescence Correlation Spectroscopy (FCS) of HC18, WC14, and FC16 tBLMs. The enhanced biological relevance of the 80% HC18 tBLMs, alluded to in the RAIRS data showing increased flexibility of the SAMs (Figure 3), does not directly address lateral phospholipid mobility (i.e., fluidity). To this end, we measured FCS on tBLMs formed with HC18, WC14, and FC16. Figure 6 displays a representative spectrum, and Table 1 summarizes the lipid diffusion coefficients D calculated from such FCS results.[32] The measurements reported here had fluorescent labels introduced into both membrane leaflets, presumably at a higher concentration in the distal membrane leaflet than in the proximal membrane leaflet, and the reported values are therefore a weighted average of the diffusive properties of these two monolayers. In an earlier, more detailed study,[32] we showed that the D value in the proximal leaflet of the WC14 tBLM is at least a factor of 2 smaller than

dx.doi.org/10.1021/la401132c | Langmuir 2013, 29, 8645−8656

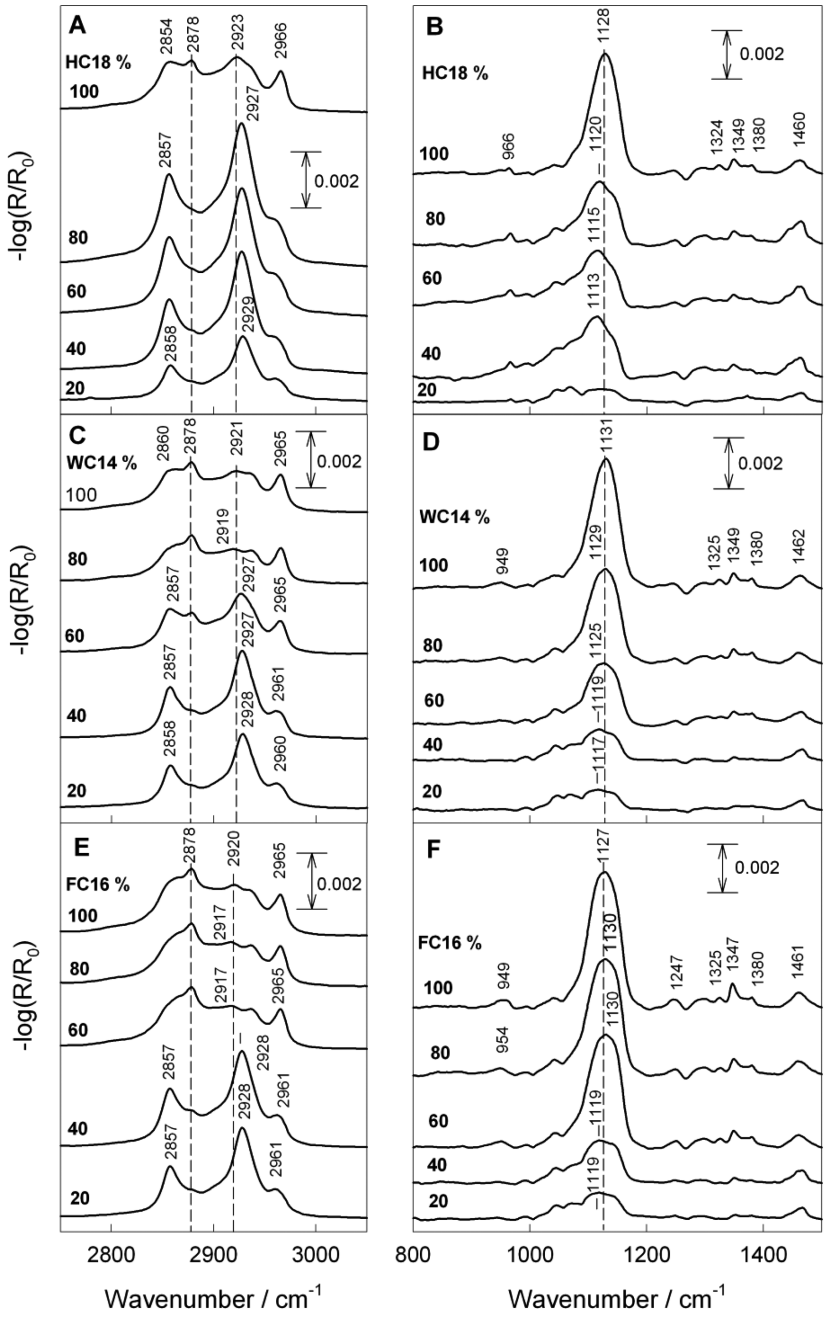

Figure 3. RAIRS spectra of the C−H and midrange regions: (A, B) for HC18/βME SAMs, respectively, (C, D) for WC14 SAMs, respectively, and (E, F) for FC16 SAMs, respectively, at tether compositions between 20 and 100%.

that in the distal leaflet. In this work, the HC18 tBLMs consistently showed compounded diffusion coefficients at ∼4 $\mu m^2/s$ (for comparison with lipid diffusion in free (black) lipid bilayers, see Part 3 in the Supporting Information), and D measured for WC14 and FC16 tBLMs did not exceed 2 $\mu m^2/s$. This indicates that lipids supported by the unsaturated alkyl chain anchor HC18 show increased lateral mobility compared to the WC14 and FC16 tBLMs.

Reconstitution of α-Hemolysin (αHL) in High- and Low-Tether-Composition HC18 and WC14 tBLMs. We investigated the reconstitution of αHL into DPhyPC-vesicle fusion-completed 80% HC18 and WC14 tBLMs and RSE-completed 20% HC18 and WC14 tBLMs. The reconstitution of αHL in tBLMs, as readily apparent from characteristic changes in the EI spectra (Bode plots),[22,24] has been found to be difficult on high-tether-composition SAMs, as observed earlier with hybrid bilayer membrane (HBM) systems.[33] Exposure to αHL resulted in EI spectral changes (Figure 7, Bode plots) consistent with αHL incorporation into the 80% HC18 tBLMs (Figure 7A) as well as for the 20% HC18 and WC14 tBLMs (data not shown; qualitatively similar to Figure 7A and that seen earlier[22]) but not for the 80% WC14 tBLMs (Figure 7B), which shows no changes.

Neutron Reflectivity (NR). NR measurements of HC18 tBLMs focused on samples that formed well-structured bilayers on HC18/βME SAMs, for which tBLM formation failed on SAMs of WC14 (ref 7) and FC16 (ref 27). Samples include tBLMs with very low tether density (12% HC18), a sample with a high proportion of anionic lipids of 40% POPG, and a tBLM prepared using vesicle fusion (Table 2 and Figure 8).

dx.doi.org/10.1021/la401132c | Langmuir 2013, 29, 8645−8656

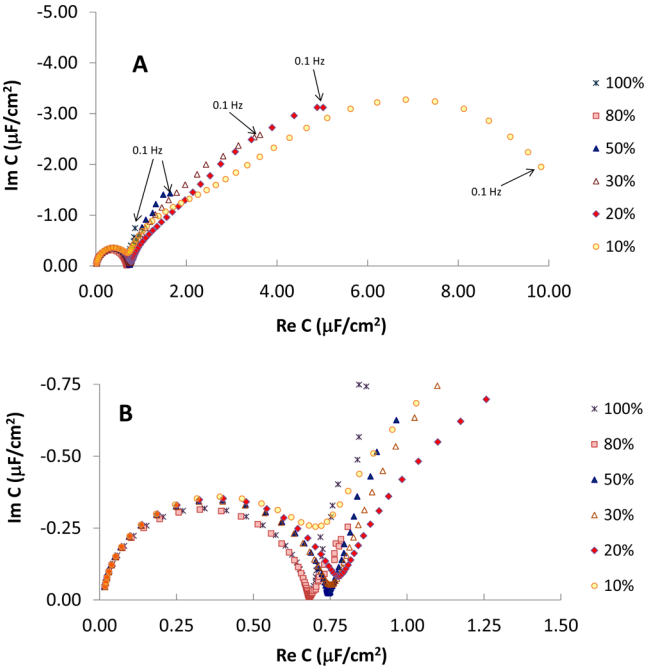

Figure 4. EI spectra of DOPC-completed HC18 tBLMs from 10 to 100% HC18. (A) Full spectra in the frequency range from 0.1 to 65,000 Hz and (B) high-frequency part of the spectra shown in pane A. Arrows indicate frequency points on EI spectra. Data normalized to a geometric surface area. The experimentally determined roughness factor of the electrodes is 1.39.

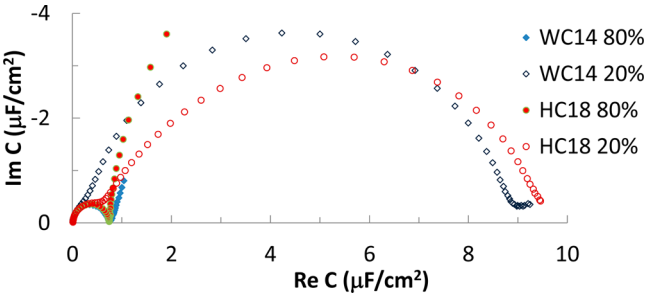

Figure 5. EI spectra of DOPC vesicle fusion on 20 and 80% WC14 and HC18 SAMs. Spectra are normalized to the geometric surface area. The experimentally determined roughness factor of the electrodes is 1.39.

(See Supporting Information for NR measurements and fitting parameters on additional HC18 tBLMs.)

The completeness of all tBLMs exceeded 90%, demonstrating the ability of HC18 to promote bilayer formation under these conditions. Using the hydrocarbon thickness values of the outer lipid leaflet, areas per free lipid molecules in the outer lipid leaflet were calculated. For single-lipid tBLMs, they are in agreement with published values for single-lipid stacked membranes at full hydration: A_0 = 72.4 Å^2 and 68.3 Å^2 for DOPC and POPC, respectively.[40] The inner lipid leaflet consistently shows a larger hydrocarbon thickness than the outer lipid leaflet, ranging from 16.1 to 17.2 Å for all measured tBLMs. This larger hydrocarbon thickness can at least partially be attributed to the ether linkage of the HC18 hydrocarbon chains to the glycerol group.[53] The hydrocarbon thickness of the inner lipid leaflet is independent of the HC18/βME ratio within the uncertainties of the measurement. The mole fraction of tether molecules in the inner lipid leaflet varies between 38 and 70%. The number of tether molecules per βME at the surface is stated with 68% confidence, in agreement with the ratio of the two molecules in the SAM-forming solutions (row 9, Table 2) except for the samples prepared from a 12% HC18 solution, where the density of tether molecules per βME at the surface is comparable to the samples made from 30% HC18 solutions.

The submembrane space of all measured samples, d_{tether} = (10 ± 2) Å, is significantly thinner than those observed for WC14 and FC16 tBLMs, (15 ± 2) and (18 ± 3) Å, respectively.[7,27] The submembrane space contains the βME molecules, the hydrated $(EO)_6$-glycerol segment of the HC18 molecule, and the lipid headgroups of the free lipids in the inner lipid leaflet. The d_{tether} values are close to the current estimates for the thickness of an unperturbed phosphocholine headgroup layer of a lipid bilayer of $d_{headgroup} \approx 9.75$ Å.[28] Therefore, the $(EO)_6$-glycerol chain of HC18 is highly disordered or exhibits a large average tilt with respect to the surface normal, a result that is in agreement with the RAIRS data (vide supra). The hydration of the submembrane space is lowest for the 80% HC18 SAM with a fill factor, f_{water}, of 7% of the total volume between the membrane and the substrate. HC18 tBLMs (12 and 30%) showed larger hydrations, f_{water} = 18−24%, with no significant differences between the various samples.

DISCUSSION

Characterization of the physicochemical, spectroscopic, and structural properties of HC18 in SAMs and completed tBLMs show this lipidic tether compound affects various aspects of molecular organization. HC18 contains a cis double bond in each of two oleoyl chains that can be expected to influence the orientation of the C_{18} chain. Our SE, CA, RAIRS, and EIS data provide convincing evidence that the HC18 SAMs and tBLMs are consistently different from those of WC14 and FC16 with more disorder in the alkyl and EO segments.

Spectroscopic Ellipsometry (SE) and Contact Angle (CA). The gradual increase in SE thickness for the HC18 SAMs from 0 to 100% HC18 (Figure 1) suggests that the HC18/βME surface concentrations correlate with the solution concentrations. The HC18/βME solution/surface concentration correlation is quantified further in the NR analysis (vide infra), albeit within relatively large uncertainties. Analogous SE increases were observed for 0 to 100% WC14 and FC16 SAMs (refs 7 and 27, respectively), though the HC18 SAMs exhibit some differences at the higher composition end (i.e., for WC14 and FC16, the SE thickness did not increase above 80% tether whereas the 100% HC18 SAM is significantly thicker than the 80 and 90% SAMs). This suggests a structural rearrangement/reorganization in the 100% HC18 SAMs, which is strongly supported by the RAIRS data (Figure 3) and discussed subsequently.

At the higher compositions, the HC18 SAMs with longer alkyl segments are thinner and less hydrophobic (Figure 1) than the corresponding WC14 SAMs (Table 1 in ref 7), whose SE and CA values are consistent with an upright structure orienting the polymethylene chains along the substrate normal.[44] The $CA_{100\%\ HC18\ SAM}$ values are similar to those of disordered alkanethiol SAMs[44] and reflect a greater exposure of the underlying methylenes to the probing liquid (water).

Interestingly, at the lower compositions the HC18 SAMs exhibit slightly higher hydrophobicity than the corresponding WC14 and FC16 SAMs. (See Figure S1 (Supporting

dx.doi.org/10.1021/la401132c | Langmuir 2013, 29, 8645−8656

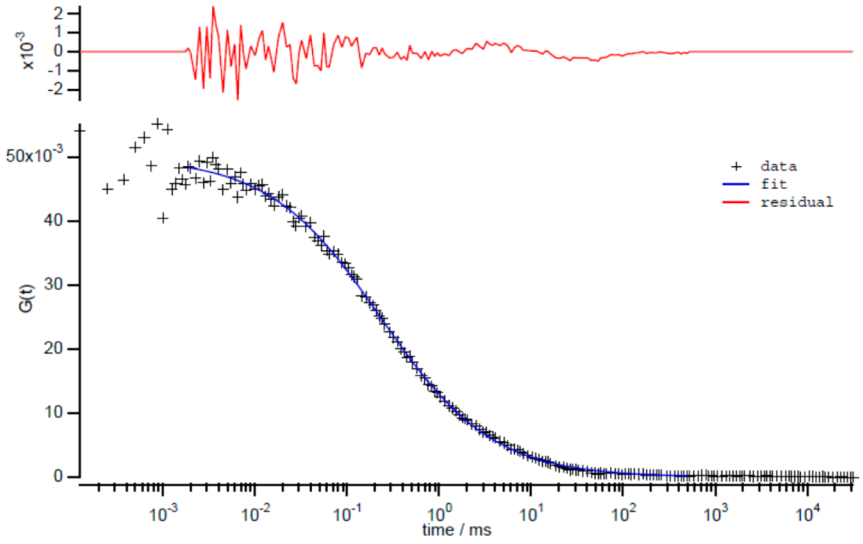

Figure 6. Representative FCS curve measured on DOPC-completed HC18 tBLM.

Table 1. Lipid Diffusivities in 70% Tether tBLMs

tether	2D diffusion coefficient, D ($\mu m^2/s$)
HC18	4.03 ± 0.21 (n = 6)
FC16	1.6 ± 0.16 (n = 5)
WC14	1.9 ± 0.18 (n = 6)

Information) for direct comparison and Table 1 in ref 7 and Table 1 in ref 27.) This suggests a more uniform surface coverage of HC18 molecules and a greater coverage of the surface by the oleoyl chains. WC14 and FC16 can be expected to cluster (i.e., form patches of aggregated molecules on the surface) to maximize the hydrophobic interactions along the saturated alkyl chains. At low tether compositions, clusters of the saturated tethers would result in significant surface areas covered with the hydrophilic βME, thereby resulting in lower CA values. A more uniform distribution of HC18 molecules would result in fewer/smaller patches of βME and greater surface coverage by the oleoyl segments, affording a higher surface energy (i.e., more hydrophobic (higher CA values)).

Reflection Absorption Infrared Spectroscopy (RAIRS). Order in SAMs may be assessed from infrared spectroscopy data. The C−H stretch region, containing the C−H stretches for the alkyl chains and the EO segments, is dominated by the bands of the alkyl chains because each tether has two of them and it is well known that prominent bands in this region are absent for EO segments in all but the most ordered SAMs.[50,51] The position of the methylene ν_a band in this region is a strong metric for order in the alkyl chains[44,54,55] appearing at 2917 cm^{-1} for highly ordered SAMs and shifting to higher wavenumbers with increasing gauche conformations along the chain (i.e., disorder). For the SAMs of all three tethers, the methylene ν_a band is found at or above 2920 cm^{-1} at all compositions (Figure 3A (HC18), 3C (WC14), and 3E (FC16)) and at 2923 cm^{-1} (100% HC18), 2921 cm^{-1} (100% WC14), and 2920 cm^{-1} (100% FC16). Thus, although the SAMs of all three tethers are disordered, the 100% FC16 SAMs are the most ordered, as might be expected for the tether with the longest saturated chains, and the HC18 SAMs are the least ordered.

The collapse of the methylene ν_a band at the higher tether compositions suggests a change in the orientation (i.e., the cant angle) of the alkyl chains. Although observed for all three tether compounds, the transition is different for HC18 (80% → 100%) relative to that for the saturated analogues (40% → 60%). A prominent methylene stretching ν_a band suggests a cant angle similar to that found for alkane thiols on Au, whereas the attenuation of this band is indicative of a smaller cant angle, as is the case for alkane thiols on Ag.[44] As the tether composition increases, lateral interactions between tether compounds should increase and the alkyl segments, decoupled from the Au surface, should be able to adopt an orientation more along the substrate normal (i.e., an upright structure (smaller cant angle), consistent with the CA values (Figure 1)). HC18, with a propensity for a more uniform surface coverage (CA data) and weaker nearest-neighbor interactions, can be expected to require a higher surface concentration for such a transition, as is observed.

The bands in the midrange region are principally those of the EO segment.[48,49] For the 100% SAMs, the ν_{as}(C−O−C) at (1129 ± 2) cm^{-1} (top spectra in Figure 3B,D,F) indicates a lack of order over any significant length scale.[50,52] The spectra of the mixed SAM compositions exhibit the ν_{as}(C−O−C) bands at lower wavenumbers, 1113 to 1119 cm^{-1} (lower spectra in Figure 3B,D,F) and are significantly broadened, suggesting a distribution of orientations and conformations[56] as might be expected with decreasing tether surface concentrations. Within this distribution of orientations and conformations for the OEO segment, the folded chain conformation (FCC)[48] (7/2 helix oriented normal to the substrate) is precluded because the bands at 1345 ± 2, 1243 ± 2, and 966 ± 2 cm^{-1} are not observed. Other "coiled" conformations, as described for previous tether compounds[56] and/or the possibility of the EO segment in the extended chain conformation (ECC), are distinct possibilities. In both cases, these conformations would give rise to shifts of the ν_{as}(C−O−C) band maximum to lower wavenumbers, as is observed.[48] It is noteworthy that for all of the mixed HC18 SAM compositions the maxima in ν_{as}(C−O−C) bands are consistently observed at 6−10 cm^{-1} lower wavenumbers relative to those of the corresponding WC14 and FC16 mixed SAMs. A more even distribution of HC18 on the surface, as discussed above, would allow more room for the ECC or coiled conformation, giving rise to a more pronounced

dx.doi.org/10.1021/la401132c | Langmuir 2013, 29, 8645−8656

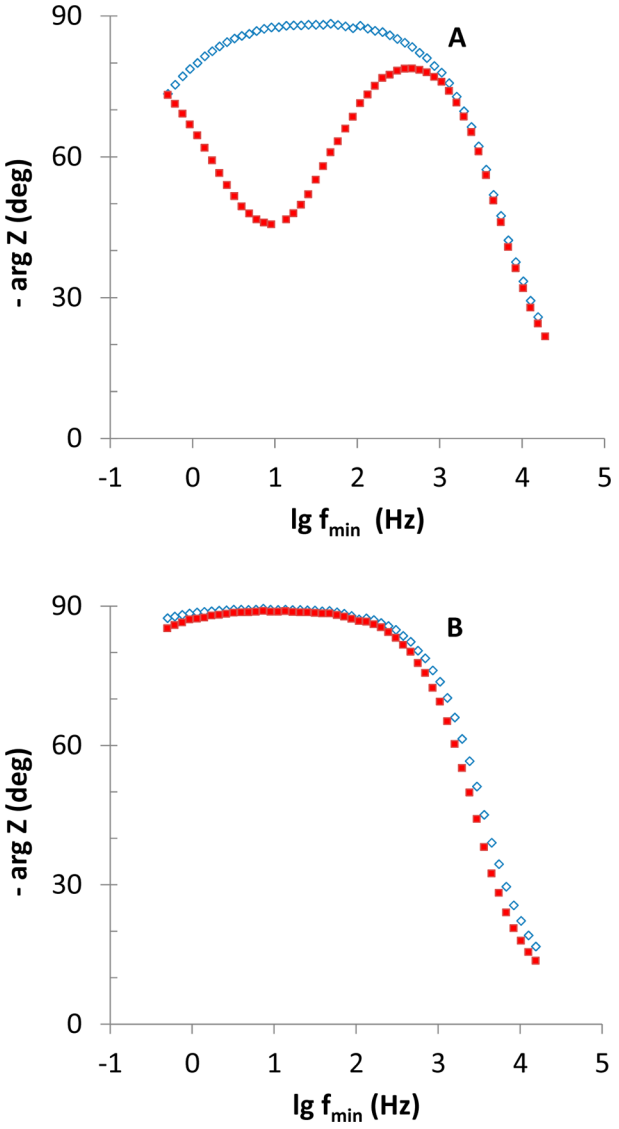

Figure 7. EI Bode spectra of tBLMs at 80% tether content, completed with DPhyPC by vesicle fusion, before incubation (open diamonds) and after incubation (filled squares) with 140 nM αHL for 60 min. (A) HC18 tBLM and (B) on WC14 tBLM.

shift in the ν_{as}(C−O−C) band position and a thinner submembrane reservoir, as indicated in the NR results.

The 100% FC16 SAMs, with the most order in the alkyl chains (Figure 3F), have some FCC order in the EO segment. A discernible band at 1347 cm^{-1} (Figure 3F, top spectrum) is evident; however, it is attenuated compared to that of OEO SAMs that have the entire EO segment in the 7/2 helical conformation.[50] This suggests that order in the alkyl segment may influence the order in the EO segment for this type of tether compound.

Electrochemical Impedance Spectroscopy (EIS). SAM capacitance (C_{SAM}) values and the dielectric constants obtained from them depend on film composition, and are especially sensitive to the presence of dipolar molecules. C_{SAM} values (Table 3) can be derived from the complex capacitance plots (Figure 2), which upon modeling yield the constant phase element (CPE) coefficient and exponent. The CPE coefficient, Q_{SAM}, which determines the impedance $Z_Q = (Q_{SAM})^{-1}(i\omega)^{-\alpha}$, can be considered to be the capacitance of the dielectric layer formed by the anchor molecules if $\alpha \rightarrow 1$, where i is the complex unit, $\omega = 2\pi f$, f is the frequency in Hz, and α is the CPE exponent. Fits to a $Q_{SAM}(R_{sol}C_{stray})$ model, written here using the Boukamp notation,[57] show α to be close to 1 (Table 3), validate the approximate equality Q_{SAM} (μF·s$^{(1-\alpha)}$ cm^{-2}) ≈ C_{SAM} (μF·cm^{-2}) and give the C_{SAM} values, from which the dielectric constants (ε) are calculated. Taking into account the nearly ideal capacitive features of the EI spectra and assuming a Helmholtz plane capacitor model of the interface, we may write for the capacitance ratio

$$\frac{C_{SAM,HC18}}{C_{SAM,WC14}} = \frac{\varepsilon_{HC18}}{\varepsilon_{WC14}} \times \frac{d_{WC14}}{d_{HC18}} \quad (1)$$

Using the C_{SAM} values for the 70% HC18 and WC14 SAMs and SE thickness values (~2.3 nm for HC18 (Figure 1) and ~2.8 nm for WC14 (ref 7)), one obtains $\varepsilon_{HC18} \approx 5.6 \times \varepsilon_{WC14}$. A similar comparison of the 70% HC18 and FC16 SAMs (d = 4.5 nm (ref 27)) gives approximately the same result, $\varepsilon_{HC18} \approx 3.5 \times \varepsilon_{FC16}$. The higher ε_{HC18} values indicate an increased concentration of dipolar molecules, presumably water, in the surface layer populated with HC18 as compared to WC14 and FC16, respectively, and is evidence of increased disorder in the higher-tether-concentration HC18 SAMs, consistent with our SE, CA, and IR data and likely the basis of the increased FCS diffusion coefficients (Table 1).

A different situation was observed for the 30% SAMs, where one obtains $\varepsilon_{HC18} \approx \varepsilon_{WC14}$ and $\varepsilon_{HC18} \approx 0.7 \times \varepsilon_{FC16}$ using eq 1, the calculated C_{SAM} values (Table 3), and SE thickness values of $d \approx 1.8$ nm for HC18 (Figure 1), $d \approx 1.6$ nm for WC14 (ref 7), and $d \approx 2.1$ nm for FC16 (ref 27), respectively. These estimates suggest that the dielectric environments are essentially independent of the tether at this concentration, presumably because of the dominance of solvent molecules at the interphase.

The evolution of EI spectral features for the DOPC-completed HC18 tBLMs at different tether compositions (Figure 4) may be rationalized by using a recent theoretical framework.[58] A defect-free tBLM should exhibit a plot in the complex capacitance plane in which all spectral points are confined to a perfect semicircle spanning from $Re\ C \rightarrow 0$ ($f \rightarrow \infty$) to $Re\ C \rightarrow C_{tBLM}$ ($f \rightarrow 0$), where $C_{tBLM} = 1/(1/C_m + 1/C_H)$, C_m is the bilayer membrane capacitance and where C_H is the Helmholtz capacitance. Defects in tBLMs give rise to low-frequency features in the EI spectra such as lines, semicircles, or combinations thereof.[12] Several physical factors are responsible for the development of these features, most importantly, the defect density (N_{def}). Other parameters are the defect size (r_0), the thickness of the submembrane layer (d_{sub}) that separates the bilayer and the solid support, the specific resistance (ρ) of the submembrane layer, and C_H. The low-frequency "tails" seen in Figure 4A, elongating with HC18 concentration decrease, attest to the increasing number of defects in tBLMs and/or the decreasing specific resistance of the submembrane layer.[58] A submembrane resistance decrease is expected from NR data, indicating that the water (electrolyte) molar fraction increases from 7 to 18−24% with the tether percentage decreasing from 80 to 12−30%. Perturbed or overlapping double or triple semicircular features, as seen for 10% HC18 DOPC tBLMs in Figure 4A, are indicative of tBLM systems with significantly different lateral defect densities or when polydisperse defect sizes coexist.[12] The EIS features in Figure 4 demonstrate an

dx.doi.org/10.1021/la401132c | Langmuir 2013, 29, 8645−8656

Table 2. Fit Parameters and Derived Properties Obtained from the Neutron Data Analysis[a]

parameter	DOPC HC18/βM E = 12/88 RSE	DOPC HC18/βM E = 80/20 RSE	DOPC HC18/βME = 30 /70 vesicle fusion	POPC-d_{31} HC18/βM E = 12/88 RSE	POPC/POPG = 60/40 HC18/βME = 30/70 RSE
best-fit χ^2	1.21	2.40	2.86	1.32	1.38
			derived properties		
area per lipid in the outer bilayer leaflet, A_0/Å^2	$73.3_{-5.7}^{+7.9}$	$76.5_{-10.7}^{+10.1}$	$70.7_{-1.4}^{+1.4}$	$68.2_{-2.0}^{+2.1}$	$97.3_{-4.3}^{+5.5}$
water fraction in submembrane space f_{water}	$0.19_{-0.04}^{+0.04}$	$0.07_{-0.06}^{+0.06}$	$0.21_{-0.02}^{+0.02}$	$0.24_{-0.02}^{+0.02}$	$0.18_{-0.03}^{+0.03}$
			membrane fit parameters		
tether length, d_{tether}/Å	$9.4_{-0.7}^{+1.1}$	$8.2_{-1.4}^{+1.4}$	$11.3_{-0.2}^{+0.2}$	$13.2_{-0.4}^{+0.4}$	$11.4_{-0.6}^{+0.5}$
surface-proximal hydrocarbon chain length d_{lipid1}/Å	$16.7_{-1.1}^{+1.1}$	$17.3_{-1.4}^{+1.0}$	$16.1_{-0.3}^{+0.4}$	$17.0_{-0.6}^{+0.7}$	$17.0_{-0.5}^{+0.6}$
surface-distal hydrocarbon chain length d_{lipid1}/Å	$13.3_{-1.3}^{+1.2}$	$12.7_{-1.5}^{+2.1}$	$13.8_{-0.3}^{+0.3}$	$13.6_{-0.4}^{+0.4}$	$9.5_{-0.6}^{+0.5}$
molar fraction of tether in inner lipid leaflet, nf_{tether}	$0.38_{-0.21}^{+0.31}$	$0.60_{-0.46}^{+0.23}$	$0.53_{-0.18}^{+0.22}$	$0.70_{-0.02}^{+0.02}$	$0.64_{-0.20}^{+0.22}$
tether surface density, ρ_{tether}/ molecules per 100 Å^2	$0.59_{-0.32}^{+0.47}$	$0.97_{-0.72}^{+0.37}$	$0.85_{-0.28}^{+0.34}$	$1.27_{-0.03}^{+0.03}$	$1.11_{-0.30}^{+0.35}$
number of tether per βME, $n_{\beta ME}$	$0.53_{-0.33}^{+2.80}$	$2.0_{-1.6}^{+8.0}$	$0.42_{-0.18}^{+0.35}$	$0.59_{-0.06}^{+0.13}$	$0.63_{-0.26}^{+0.48}$
completeness of bilayer, $vf_{bilayer}$	$0.92_{-0.01}^{+0.02}$	$0.93_{-0.02}^{+0.02}$	$1.00_{-0.01}^{+0.00}$	$0.99_{-0.01}^{+0.01}$	$1.00_{-0.02}^{+0.00}$

[a]Confidence limits (~68%) were obtained using a Monte Carlo resampling technique.[27] For a complete list of fit parameters, see the Supporting Information.

inverse relationship between the defectiveness and tether density in the tBLMs.

Vesicle fusion occurs differently on the HC18 and the WC14 SAMs (Figure 5). At low WC14 concentration (20%), the EIS spectra after interaction with DOPC vesicles (blue open diamonds) exhibit marginal differences from that of the as-prepared 20% WC14 SAMs [Figure 5, ref 7 (20% WC14) and Figure 2A (30% WC14)] with only a small portion of the semicircular patch visible at the high-frequency end. In contrast, for 20% HC18, the spectrum after interaction with the DOPC vesicles (red open circles) exhibits over half of the high-frequency semicircular feature, indicating that less-defective tBLMs may be generated via the vesicle fusion process. At high concentrations (80%), both SAMs form tBLMs via vesicle fusion, as seen from the nearly perfect high-frequency semicircular part of the complex capacitance plots (Figure 5 (filled red circles and blue diamonds)).

Such high-tether-density tBLMs, which are approaching the earlier HBM systems, may not exhibit enough fluidity to reconstitute membrane proteins functionally.[33] We estimate the 2D diffusion coefficients, D (μm^2/s), of fluorescently labeled DOPC in our high-tether-density tBLMs (Table 1) from FCS data, such as that shown for HC18 (Figure 6). DOPC exhibits a significantly higher 2D diffusion coefficient relative to that of saturated WC14 and FC16 ($D_{HC18\ tBLMs} \geq 2D_{WC14\ tBLMs}$ and $2D_{FC16\ tBLMs}$).

The biological relevance of the increased fluidity of the high-tether-density (80%) DPhyPC vesicle-fused HC18 tBLMs was demonstrated by the reconstitution of αHL (Figure 7A). The property of the reconstitution of αHL and, by extension, other integral membrane proteins (IMPs) over a broader range of tether density (20 to 80%) that includes the more electrically insulating high-tether-density compositions increases the potential usefulness of HC18-based tBLMs in biosensor applications.

NR data shows that the submembrane reservoir in HC18 tBLMs is thinner and holds less water than the WC14 tBLMs ($d_{sub,WC14}$ = 1.5 ± 0.2 nm (ref 7) vs $d_{tether,HC18}$ = 1.0 ± 0.2 nm (Table 2)) despite identical EO segments. This has consequences for the electrical properties of the membrane because the specific resistance of the submembrane space affects the total impedance of a defect.[58,59] This contribution increases with the specific resistance and becomes dominant for large water-filled defects. Our results and data published earlier by others[59] point to a higher specific resistance of an electrolyte confined in the submembrane space as compared to that of the same electrolyte in the bulk. This is the consequence of reduced ion mobility and differences in the dielectric environment in the confined space and in the bulk. Confinement of the EO segments to the smaller submembrane volume in the HC18 tBLMs localizes the EO segments closer to the solid surface. This is consistent with the observed small capacitances of HC18 SAMs and, as recent theoretical work predicts,[58] results in higher resistances of the HC18 tBLMs, despite their lower hydrophobic membrane thickness.

The more disordered HC18/βME SAMs (SE, CA, and RAIRS data) support the formation of electrically insulating, low-defect tBLMs at <20% tether compositions (EIS data), lower than WC14 and FC16 (30% tether).[7,27] However, at all tether compositions, the HC18 tBLMs consistently show better electrical parameters than do WC14 and FC16 tBLMs (EIS data). Importantly, the HC18 tBLMs are readily completed by vesicle fusion over a broad range of tether composition, affording distinct advantages for the incorporation of IMPs and alleviating restrictions in the RSE method (i.e., ethanol-insoluble lipids).

CONCLUSIONS

The new tether lipid HC18 [*Z*-20-(*Z*-octadec-9-enyloxy)-3,6,9,12,15,18,22-heptaoxatetra-cont-31-ene-1-thiol] with double bonds in its alkyl segments allows the formation of complete tBLMs on preformed HC18/βME SAMs by RSE or vesicle fusion. SE, CA, RAIRS, and EIS data lead to a consistent picture of more disorder in the HC18 SAMs that leads to enhanced bilayer fluidity in the tBLMs. The resulting membrane mimics exhibit biologically relevant fluidity and readily reconstitutes pore-forming toxin αHL at tether mole fractions of up to 80%, which is not possible with WC14 and FC16 tBLMs containing saturated alkyl segments. In addition, HC18 affords the formation of stable and complete tBLMs with

dx.doi.org/10.1021/la401132c | Langmuir 2013, 29, 8645−8656

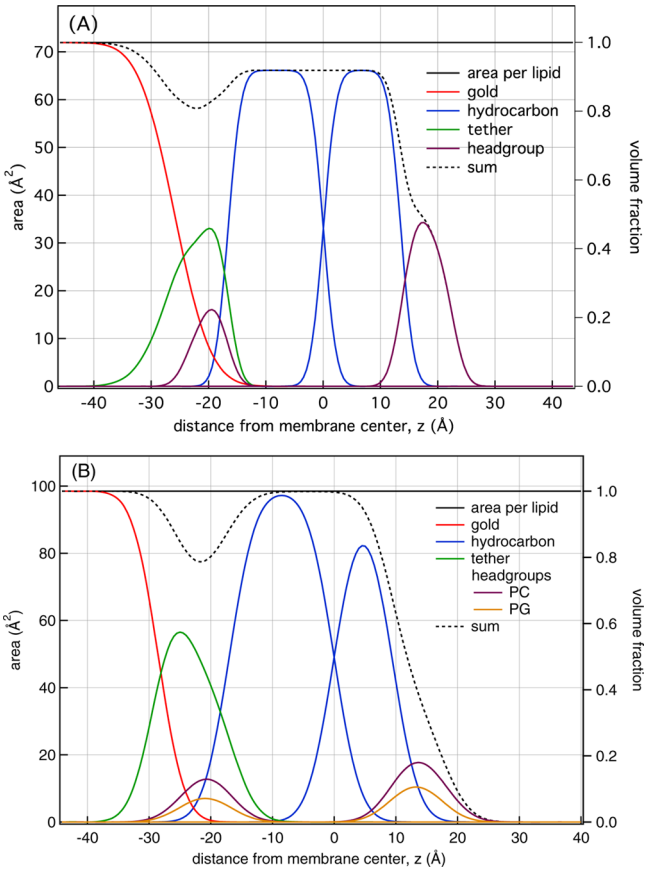

Figure 8. Volume occupancy profiles of submolecular fragments of HC18-tethered tBLMs derived from NR measurements. (A) DOPC-completed tBLM on 12% HC18 SAM. (B) tBLM completed with a lipid mixture of high anionic content, 60/40 POPC/POPG. The panels show material distributions normalized to the average areas per free phospholipid in the tBLM (left axis) and normalized to 1 (volume fraction, right axis). Colored, solid lines visualize the fractional in-plane filling of space by different molecular moieties as indicated. Dashed lines show the sum profiles of the organic components of the tBLM, with the implication that the distance between the full space (solid black line) and the dashed line indicates space filled with buffer. See the Supporting Information for a complete set of volume occupancy profiles for all measured samples.

high anionic lipid content (e.g., 40% POPG/POPC). We demonstrate that the 80% HC18 tBLMs appear to be optimal for practical applications such as biosensor applications where high electrical insulation and the possibility of protein (peptide) reconstitution are imperative, and we believe that the HC18 tBLMs are an interesting model system for biological membranes.

■ ASSOCIATED CONTENT

Supporting Information

Additional contact angle data/analysis and neutron reflectivity data/additional fitting parameters. This material is available free of charge via the Internet at http://pubs.acs.org.

■ AUTHOR INFORMATION

Corresponding Author

*E-mail: vanderah@ibbr.umd.edu. Tel: +1-240-314-6266.

Present Address

[○]Department of Quantum Electronics, Vilnius University, Vilnius LT-08662, Lithuania.

Notes

The authors declare no competing financial interest.

■ ACKNOWLEDGMENTS

This work was supported, in part, by the National Institute of General Medical Sciences (1R01 GM101647) and the Research Council of Lithuania (MIP-096/2011) and performed, in part, at the NIST Center for Nanoscale Science and Technology. F.H. was supported by the Department of Commerce (MSE grant 70NANB8H8009), and H.C. was supported by a summer undergraduate research fellowship (SURF) in 2009 at NIST.

■ REFERENCES

(1) Brian, A. A.; McConnell, H. M. Allogenic Stimulation of Cytotoxic T-Cells by Supported Planar Membranes. *Proc. Natl. Acad. Sci. U.S.A.* **1984**, *81*, 6159−6163.

(2) Tamm, L. K.; McConnell, H. M. Supported Phospholipid-Bilayers. *Biophys. J.* **1985**, *47*, 105−113.

(3) Sackmann, E. Supported Membranes: Scientific and Practical Applications. *Science* **1996**, *271*, 43−48.

(4) Castellana, E. T.; Cremer, P. S. Solid Supported Lipid Bilayers: From Biophysical Studies to Sensor Design. *Surf. Sci. Rep.* **2006**, *61*, 429−444.

(5) Knoll, W.; Bender, K.; Foerch, R.; Frank, C.; Goetz, H.; Heibel, C.; Jenkins, T.; Jonas, U.; Kibrom, A.; Kuegler, R.; Naumann, C. A.; Naumann, R.; Reisinger, A.; Ruehe, J.; Schiller, S.; Sinner, E.-K. Polymer-Tethered Bimolecular Lipid Membranes. *Adv. Polym. Sci.* **2010**, *224*, 87−111.

(6) Lang, H.; Duschl, C.; Vogel, H. A New Class of Thiolipids for the Attachment of Lipid Bilayers on Gold Surfaces. *Langmuir* **1994**, *11*, 197−210.

(7) McGillivray, D. J.; Valincius, G.; Vanderah, D. J.; Febo-Ayala, W.; Woodward, J. T.; Heinrich, F.; Kasianowicz, J. J.; Lösche, M. Molecular-Scale Structural and Functional Characterization of Sparsely-Tethered Lipid Bilayers. *Biointerphases* **2007**, *2*, 21−33.

(8) Purrucker, O.; Fortig, A.; Jordan, R.; Tanaka, M. Supported Membranes with Well-Defined Polymer Tethers-Incorporation of Cell Receptors. *ChemPhysChem* **2004**, *5*, 327−335.

(9) Wagner, M. L.; Tamm, L. K. Tethered Polymer-Supported Planar Lipid Bilayers for Reconstitution of Integral Membrane Proteins:

Table 3. Comparison of the Electrical Parameters of SAMs

	30% SAM		70% SAM	
tether	C_{SAM}, μF/cm^2 [a]	α	C_{SAM}, μF/cm^2 [a]	α
HC18[b]	6.56 ± 0.20	0.996 ± 0.001	6.23 ± 0.20	0.996 ± 0.001
WC14[c]	7.18 ± 0.21	0.996 ± 0.001	0.92 ± 0.03	0.997 ± 0.001
FC16[d]	7.56 ± 0.19	0.996 ± 0.0004	0.90 ± 0.04	0.993 ± 0.002

[a]EIS data was fitted to a $Q_{SAM}(R_sC_{stray})$ model in the frequency interval from 25 to 65 000 Hz. The approximate equality $Q_{SAM} \approx C_{SAM}$ was assumed from the closeness of α to 1. Presented C_{SAM} values are normalized to the geometric surface area. To obtain C_{SAM} values normalized to the real surface area, divide by the roughness coefficient 1.39. [b]Average of 14 samples for 30% SAM and average of 13 samples for 70% SAM. [c]Average of 10 samples for 30% SAM and average of 5 samples for 70% SAM. [d]Average of 12 samples for 30% SAM and average of 6 samples for 70% SAM.

Silane-Polyethyleneglycol-Lipid as a Cushion and Covalent Linker. *Biophys. J.* **2000**, *79*, 1400−1414.
(10) Atanasov, V.; Knorr, N.; Duran, R. S.; Ingebrandt, S.; Offenhäusser, A.; Knoll, W.; Köper, I. Membrane on a Chip: A Functional Tethered Lipid Bilayer Membrane on Silicon Oxide Surfaces. *Biophys. J.* **2005**, *89*, 1780−1788.
(11) Becucci, L.; Innocenti, M.; Salvietti, E.; Rindi, A.; Pasquini, I.; Vassalli, M.; Foresti, M. L.; Guidelli, R. Potassium Ion Transport by Gramicidin and Valinomycin Across a Ag(111)-Supported Tethered Bilayer Lipid Membrane. *Electrochim. Acta* **2008**, *53*, 6372−6379.
(12) Kwak, K. J.; Valincius, G.; Liao, W.-C.; Hu, X.; Wen, X.; Lee, A.; Yu, B.; Vanderah, D. J.; Lu, W.; Lee, L. J. Formation and Finite Element Analysis of Tethered Bilayer Lipid Structures. *Langmuir* **2010**, *26*, 18199−18208.
(13) Chung, M.; Lowe, R. D.; Chan, Y.-H. M.; Ganesan, P. V.; Boxer, S. G. Formation and Analysis of Topographical Domains between Lipid Membranes Tethered by DNA Hybrids of Different Lengths. *J. Struct. Biol.* **2009**, *168*, 190−199.
(14) Kibrom, A.; Roskamp, R. F.; Jonas, U.; Menges, B.; Knoll, W.; Paulsen, H.; Naumann, R. L. C. Hydrogel-Supported Protein-Tethered Bilayer Lipid Membranes: A New Approach toward Polymer-Supported Lipid Membranes. *Soft Matter* **2011**, *7*, 237−246.
(15) Terrettaz, S.; Mayer, M.; Vogel, H. Highly Electrically Insulating Tethered Lipid Bilayers for Probing the Function of Ion Channel Proteins. *Langmuir* **2003**, *19*, 5567−5569.
(16) Valincius, G.; Heinrich, F.; Budvytyte, R.; Vanderah, D. J.; McGillivray, D. J.; Sokolov, Y.; Hall, J. E.; Lösche, M. Soluble amyloid β-oligomers affect dielectric membrane properties by bilayer insertion and domain formation: Implications for cell toxicity. *Biophys. J.* **2008**, *95*, 4845−4861.
(17) Merzlyakov, M.; Li, E.; Hristova, K. Directed Assembly of Surface-Supported Bilayers with Transmembrane Helices. *Langmuir* **2006**, *22*, 1247−1253.
(18) Jeuken, L. J. C.; Connell, S. D.; Henderson, P. J. F.; Gennis, R. B.; Evans, S. D.; Bushby, R. J. Redox Enzymes in Tethered Membranes. *J. Am. Chem. Soc.* **2006**, *128*, 1711−1716.
(19) Vockenroth, I. K.; Atanasova, P. P.; Jenkins, A. T. A.; Köper, I. Incorporation of Alpha-Hemolysin in Different Tethered Bilayer Lipid Membrane Architectures. *Langmuir* **2008**, *24*, 496−502.
(20) Andersson, M.; Okeyo, G.; Wilson, D.; Keizer, H.; Moe, P.; Blount, P.; Fine, D.; Dodabalapur, A.; Duran, R. S. Voltage-Induced Gating of the Mechanosensitive MscL Ion Channel Reconstituted in a Tethered Lipid Bilayer Membrane. *Biosens. Bioelectron.* **2008**, *23*, 919−923.
(21) Jadhav, S. R.; Sui, D.; Garavito, R. M.; Worden, R. M. Fabrication of Highly Insulating Tethered Bilayer Lipid Membrane Using Yeast Cell Membrane Fractions for Measuring Ion Channel Activity. *J. Colloid Interface Sci.* **2008**, *322*, 465−472.
(22) McGillivray, D. J.; Valincius, G.; Heinrich, F.; Robertson, J. W. F.; Vanderah, D. J.; Febo-Ayala, W.; Ignatjev, I.; Lösche, M.; Kasianowicz, J. J. Structure of Functional Staphylococcus aureus alpha-Hemolysin Channels in Tethered Bilayer Lipid Membranes. *Biophys. J.* **2009**, *96*, 1547−1553.
(23) Sevin-Landais, A.; Rigler, P.; Tzartos, S.; Hucho, F.; Hovius, R.; Vogel, H. Functional Immobilisation of the Nicotinic Acetylcholine Receptor in Tethered Lipid Membranes. *Biophys. Chem.* **2000**, *85*, 141−152.
(24) Cornell, B. A.; Braach-Maksvytis, V. L. B.; King, L. B.; Osman, P. D. J.; Raguse, B.; Wieczorek, L.; Pace, R. J. A Biosensor That Uses Ion-Channel Switches. *Nature* **1997**, *387*, 580−583.
(25) Sumino, A.; Dewa, T.; Takeuchi, T.; Sugiura, R.; Sasaki, N.; Misawa, N.; Tero, R.; Urisu, T.; Gardiner, A. T.; Cogdell, R. J.; Hashimoto, H.; Nango, M. Construction and Structural Analysis of Tethered Lipid Bilayer Containing Photosynthetic Antenna Proteins for Functional Analysis. *Biomacromolecules* **2011**, *12*, 2850−2858.
(26) Bayley, H.; Cremer, P. S. Stochastic Sensors Inspired by Biology. *Nature* **2001**, *413*, 226−230.
(27) Heinrich, F.; Ng, T.; Vanderah, D. J.; Shekhar, P.; Mihailescu, M.; Nanda, H.; Lösche, M. A New Lipid Anchor for Sparsely Tethered Bilayer Lipid Membranes. *Langmuir* **2009**, *25*, 4219−4229.
(28) Shekhar, P.; Nanda, H.; Lösche, M.; Heinrich, F. Continuous Distribution Model for the Investigation of Complex Molecular Architectures near Interfaces with Scattering Techniques. *J. Appl. Phys.* **2011**, *110*, 102216-1−102216-12.
(29) Naumann, R.; Schiller, S. M.; Giess, F.; Grohe, B.; Hartman, K. B.; Karcher, I.; Köper, I.; Lubben, J.; Vasilev, K.; Knoll, W. Tethered Lipid Bilayers on Ultraflat Gold Surfaces. *Langmuir* **2003**, *19*, 5435−5443.
(30) Schiller, S. M.; Naumann, R.; Lovejoy, K.; Kunz, H.; Knoll, W. Archaea Analogue Thiolipids for Tethered Bilayer Lipid Membranes on Ultrasmooth Gold Surfaces. *Angew. Chem., Int. Ed.* **2003**, *42*, 208−211.
(31) Junghans, A.; Köper, I. Structural Analysis of Tethered Bilayer Lipid Membranes. *Langmuir* **2010**, *26*, 11035−11040.
(32) Shenoy, S.; Moldovan, R.; Fitzpatrick, J.; Vanderah, D. J.; Deserno, M.; Lösche, M. In-Plane Homogeneity and Lipid Dynamics in Tethered Bilayer Lipid Membranes (tBLMs). *Soft Matter* **2010**, *6*, 1263−1274.
(33) Glazier, S. A.; Vanderah, D. J.; Plant, A. L.; Bayley, H.; Valincius, G.; Kasianowicz, J. J. Reconstitution of the Pore-Forming Toxin Alpha-Hemolysin in Phospholipid/18-Octadecyl-1-Thiahexa(Ethylene Oxide) and Phospholipid/*n*-Octadecanethiol Supported Bilayer Membranes. *Langmuir* **2000**, *16*, 10428−10435.
(34) He, L.; Robertson, J. W. F.; Li, J.; Kärcher, I.; Schiller, S. M.; Knoll, W.; Naumann, R. Tethered Bilayer Lipid Membranes Based on Monolayers of Thiolipids Mixed with a Complementary Dilution Molecule. 1. Incorporation of Channel Peptides. *Langmuir* **2005**, *21*, 11666−11672.
(35) Certain commercial equipment, instruments, or materials are identified in this Article to specify the experimental procedure adequately. Such identification is not intended to imply recommendation or endorsement by the National Institute of Standards and Technology nor is it intended to imply that the materials or equipment are necessarily the best available for that purpose.
(36) Olah, G. A.; Gupta, B. G. B.; Malhotra, R.; Narang, S. C. Synthetic Methods and Reactions. 81. Chlorotrimethylsilane-Lithium Bromide and Hexamethyldisilane-Pyridinium Bromide Perbromide − Effective and Selective Reagents for the Conversion of Alkyl(cycloalkyl and arylalkyl) Alcohols into Bromides. *J. Org. Chem.* **1980**, *45*, 1638−1639.
(37) Dura, J. A.; Pierce, D. J.; Majkrzak, C. F.; Maliszewskyj, N. C.; McGillivray, D. J.; Lösche, M.; O'Donovan, K. V.; Mihailescu, M.; Perez-Salas, U.; Worcester, D. L.; White, S. H. AND/R: Advanced Neutron Diffractometer/Reflectometer for Investigation of Thin Films and Multilayers for the Life Sciences. *Rev. Sci. Instrum.* **2006**, *77*, 74301−743011.
(38) Wiener, M. C.; White, S. H. Fluid Bilayer Structure Determination by the Combined use of X-ray and Neutron diffraction. 2. Composition-Space Refinement Method. *Biophys. J.* **1991**, *59*, 174−185.
(39) Vaknin, D.; Kjaer, K.; Als-Nielsen, J.; Lösche, M. Structural-Properties of Phosphatidylcholine in a Monolayer at the Air-Water Interface − Neutron Reflection Study and Reexamination of X-ray Reflection Measurements. *Biophys. J.* **1991**, *59*, 1325−1332.
(40) Kucerka, N.; Tristram-Nagle, S.; Nagle, J. F. Structure of Fully Hydrated Fluid Phase Lipid Bilayers with Monounsaturated Chains. *J. Membr. Biol.* **2005**, *208*, 193−202.
(41) Nagle, J. F.; Tristram-Nagle, S. Structure of Lipid Bilayers. *Biochim. Biophys. Acta* **2000**, *1469*, 159−195.
(42) Kirby, B. J.; Kienzle, P. A.; Maranville, B. B.; Berk, N. F.; Krycka, J.; Heinrich, F.; Majkrzak, C. F. Phase-Sensitive Specular Neutron Reflectometry for Imaging the Nanometer Scale Composition Depth Profile of Thin-Film Materials. *Curr. Opin. Colloid Interface Sci.* **2012**, *17*, 44−53.

(43) Haustein, E.; Schwille, P. Fluorescence Correlation Spectroscopy: Novel Variations of an Established Technique. *Annu. Rev. Biophys. Biomol. Struct.* **2007**, *36*, 151−169.
(44) Laibinis, P. E.; Whitesides, G. M.; Allara, D. L.; Tao, Y.-T.; Parikh, A. N.; Nuzzo, R. G. Comparison of the Structures and Wetting Properties of Self-Assembled Monolayers of Normal-Alkanethiols on the Coinage Metal-Surfaces, Cu, Ag, Au. *J. Am. Chem. Soc.* **1991**, *113*, 7152−7167.
(45) Harder, P.; Grunze, M.; Dahint, R.; Whitesides, G. M.; Laibinis, P. E. Molecular Conformation in Oligo(ethylene glycol)-Terminated Self-Assembled Monolayers on Gold and Silver Surfaces Determines Their Ability to Resist Protein Adsorption. *J. Phys. Chem. B* **1998**, *102*, 426−436.
(46) Malysheva, L.; Onipko, A.; Valiokas, R.; Liedberg, B. Spectroscopic Characterization and Modeling of Methyl- and Hydrogen-Terminated Oligo(ethylene glycol) Self-Assembled Monolayers. *J. Phys. Chem. A* **2005**, *109*, 7788−7796.
(47) Valiokas, R.; Malysheva, L.; Onipko, A.; Lee, H. H.; Ruželė, Ž.; Svedhem, S.; Svensson, S. C. T.; Gelius, U.; Liedberg, B. On the Quality and Structural Characteristics of Oligo(ethylene glycol) Assemblies on Gold: An Experimental and Theoretical Study. *J. Electron Spectrosc. Relat. Phenom.* **2009**, *172*, 9−20.
(48) Kobayashi, M.; Sakashita, M. Morphology Dependent Anamolous Frequency-Shifts of Infrared-Absorption Bands of Polymer Crystals − Interpretation in terms of Transition Dipole Dipole Coupling Theory. *J. Chem. Phys.* **1992**, *96*, 748−760.
(49) Miyazawa, T.; Fukushima, K.; Ideguchi, Y. Molecular Vibrations and Structure of High Polymers III. Polarized Infrared Spectra, Normal Vibrations, and Helical Conformation of Polyethylene Glycol. *J. Chem. Phys.* **1962**, *37*, 2764−2776.
(50) Vanderah, D. J.; Arsenault, J.; La, H.; Gates, R. S.; Silin, V.; Meuse, C. W.; Valincius, G. Structural Variations and Ordering Conditions for the Self-Assembled Monolayers of HS-$(CH_2CH_2O)_{3-6}CH_3$. *Langmuir* **2003**, *19*, 3752−3756.
(51) Vanderah, D. J.; Gates, R. S.; Silin, V.; Zeiger, D. N.; Woodward, J. T.; Meuse, C. W.; Nickel, B.; Valincius, G. Isostructural Self-Assembled Monolayers. 1. Octadecyl 1-Thiaoligo(ethylene oxides). *Langmuir* **2003**, *19*, 2612−2620.
(52) For compounds of the general type $HS(EO)_xR$, where $x > 5$ and $R = C_nH_{2n+1}$ (n = 1 to 18), EO segments order in a $^7/_2$ helical conformation (ref 51). On Au, these segments are oriented along the substrate normal in the folded chain conformation (FCC), with the oxygen atoms co-located parallel to the substrate. The spectral characteristics of the FCC have been described in detail[48] and are characterized by the prominent ν_{as}(C−O−C) band at 1118 cm^{-1} [$A_2(6)$], accompanied by bands at (1345 ± 2) cm^{-1} [$A_2(4)$], (1243 ± 2) cm^{-1} [$A_2(5)$], and (966 ± 2) cm^{-1} [$A_2(7)$]. The extended chain conformation (ECC) is identical in conformation to FCC, but the chains are positioned such that the oxygen atoms are not co-located. To attain the ECC conformation on Au, a 1-mercapto-OEO compound would require a substantial cant angle (≥45°). The ECC conformation exhibits the prominent $A_2(6)$ band at 1109 cm^{-1}.[48]
(53) Guler, S. D.; Ghosh, D. D.; Pan, J.; Mathai, J. C.; Zeidel, M. L.; Nagle, J. F.; Tristram-Nagle, S. Effects of Ether vs. Ester Linkage on Lipid Bilayer Structure and Water Permeability. *Chem. Phys. Lipids* **2009**, *160*, 33−44.
(54) Parikh, A. N.; Allara, D. Quantitative-Determination of Molecular-Structure in Multilayered Thin-Films of Biaxial and Lower Symmetry from Photon Spectroscopies. 1. Reflection Infrared Vibrational Spectroscopy. *J. Chem. Phys.* **1992**, *96*, 927−945.
(55) Porter, M. D.; Bright, T. B.; Allara, D. L.; Chidsey, C. E. D. Spontaneously Organized Molecular Assembles. 4. Structural Characterization of Normal-Alkyl Thiol Monolayers on Gold by Optical Ellipsometry, Infrared-Spectroscopy, and Electrochemistry. *J. Am. Chem. Soc.* **1987**, *109*, 3559−3568.
(56) Leitch, J.; Kunze, J.; Goddard, J. D.; Schwan, A. L.; Faragher, R. J.; Neumann, R.; Knoll, W.; Dutcher, J. R.; Lipkowski, J. In Situ PM-IRRAS Studies of an Analogue Thiolipid Assembled on a Au(111) Electrode Surface. *Langmuir* **2009**, *25*, 10354−10363.
(57) Boukamp, B. A Nonlinear Least-Squares Fit Procedure for Analysis of Immittance Data of Electrochemical Systems. *Solid State Ionics* **1986**, *20*, 31−44.
(58) Valincius, G.; Meskauskas, T.; Ivanauskas, F. Electrochemical Impedance Spectroscopy of Tethered Bilayer Membranes. *Langmuir* **2012**, *28*, 977−990.59.
(59) Krishna, G.; Schulte, J.; Cornell, B. A.; Pace, R. J.; Osman, P. D. Tethered Bilayer Membranes Containing Ionic Reservoirs: Selectivity and Conductance. *Langmuir* **2003**, *19*, 2294−2305.